International Journal of Solids and Structures 304 (2024) 113054

Contents lists available at ScienceDirect

International Journal of Solids and Structures

journal homepage: www.elsevier.com/locate/ijsolstr

ANN based optimization of nano-beam oscillations with intermolecular forces and geometric nonlinearity

Naveed Ahmad Khan [a,b,*], Muhammad Sulaiman [c], Benzhou Lu [a,b]

[a] State Key Laboratory of Scientific and Engineering Computing, Academy of Mathematics and Systems Science, Chinese Academy of Sciences, Beijing, China
[b] School of Mathematical Sciences, University of Chinese Academy of Sciences, Beijing, China
[c] Department of Mathematics, Abdul Wali Khan University, Mardan, 23200, Pakistan

ARTICLE INFO

Keywords:
Van der Waals (VdW) force
Casimir attractions
Beam-type actuators
Kármán model
Applied voltage
Dispersion forces
Artificial intelligence

ABSTRACT

In this study, we investigate the effect of Van der Waals and Casimir forces on the mathematical model of nano-electromechanical systems (NEMS) such as nano-beam actuators that contain cantilever and double cantilever beams. The singular nonlinear boundary value problem governing the beam-type actuators, including geometric nonlinearity is solved by using an intelligent strength of feedforward artificial neural networks (ANNs) and hybridization of optimization algorithms such as arithmetic optimization algorithm (AOA) and active set algorithm (ASA). The proposed ANN-AOA-AS algorithm is employed to quantify the effect of changes in applied voltage, dispersion forces, geometric nonlinearity parameters, and initial axial strain on the deflection of the beam. Furthermore, to validate the results obtained by the proposed algorithm, statistical analyses are conducted to compare the approximate solutions with state-of-the-art methodologies available in the latest literature. In addition, performance indicators are defined such as mean square error (MSE), Nash–Sutcliffe efficiency (NSE), mean absolute deviations (MAD), root mean square error (RMSE), and Error in Nash–Sutcliffe efficiency (ENSE) to study the accuracy and efficiency of the solutions. The results show that these indicators' mean percentage values lie around 10^{-4} to 10^{-6} which reflects the perfect modeling of the approximate solutions.

1. Introduction

The beam-type electrostatic actuator system has emerged as one of the most important systems that may be employed as a critical component in the construction of models such as micro-electromechanical systems (MEMS) and nanoelectromechanical systems (NEMs), among other applications. These electrostatic nano-actuators are recently being used in developing nano-tweezers, nano-tweezers, and hydraulic actuators etc (Ke, 2006; Pelesko and Bernstein, 2002). A beam-type NEMS is made up of a conducting nano-electrode hanging over a conductor substrate. Due to the presence of electrostatic forces, when a voltage difference between the ground and the electrode is applied, the electrode deflects and attracts towards the earth. The pull-in instability occurs when the electrostatic attraction exceeds the elastic restoring moment of the NEMS and leads to contact between the two electrodes at the critical voltage, also known as the pull-in voltage (Koochi et al., 2014). In the last two decades, the micro-electromechanical systems' (MEMS) pull-in behavior without considering the nano-scale effect was studied by different researchers (Osterberg, 1995; Batra et al., 2007). Nano-scale phenomenons such as size dependency, and dispersion forces can dramatically influence the performance of nano-structures, it is because the initial spacing between the electrodes is quite small therefore, such effects have piqued the curiosity of a large number of researchers (Radi et al., 2021; Lim, 2010; Amorim et al., 2015).

To study the damping (thermoelastic) in NEMS and MEMS, researchers have used the basis of classical theory of coupled thermoelasticity. Some works based on classical theories are summarized as follows. The buckling of nano-wires was studied by Wang and Feng (2009) under the influence of surface residual stresses and surface elasticity. Wen-Hui and Ya-Pu (2003) investigate the effects of Van Der Waal forces (vdW) on the dynamical behavior of nano-scale beams. A continuum theory was developed by Gurtin and Ian Murdoch (1975), Gurtin and Murdoch (1978) to model the surface elasticity and residual surface stress to study the variations on the behavior of beam-type nanostructures. Guo and Rogerson (2003) used a two-dimensional

* Corresponding author at: State Key Laboratory of Scientific and Engineering Computing, Academy of Mathematics and Systems Science, Chinese Academy of Sciences, Beijing, China.
E-mail address: khanna@lsec.cc.ac.cn (N.A. Khan).

https://doi.org/10.1016/j.ijsolstr.2024.113054
Received 5 May 2024; Received in revised form 29 June 2024; Accepted 27 August 2024
Available online 30 August 2024

parabolic heat conduction model to investigate the thermoelastic damping and significance of energy dissipation of silicon-based MEMS beam resonators. The quality factor of the beam in state-of-the-art MEMS gyroscopes under the influence of thermoelastic damping and suspensions was studied by the Künzig et al. (2010).

In recent times, researchers have focused on studying the pull-in behavior of nanobeamns by varying Casimir force and Van der Waals attractions (Hosseini et al., 2017). Batra et al. (2008) used finite element method to simulate the instability of the micromembranes and micro-plates under the influence of Casimir force. Ramezani et al. (2008) investigates the effect of various forces on the pull-in behavior of the electrostatic nano-cantilever beam actuators by using Green's function. Liem et al. (2020) used an inverse method to predict the axial load, elastic modulus, and boundary conditions of a nanoelectromechanical system beam from a minimum of two measured natural frequencies. An experimental study was conducted by Noghrehabadi et al. (2011) using the homotopy perturbation technique (HPM) to investigate the pull-in behavior and stress field of cantilever nano-beam actuators with Van der Waals attraction. Herişanu and Marinca (2010) analytically treats the non-linear oscillations of planar, flexural large amplitude free vibrations of an inextensible cantilever beam carrying a lumped mass, and slender with rotary inertia at an intermediate position along its span. The optimal homotopy asymptotic method was utilized by Herisanu and Marinca (2018) to study the large post-buckling deformation of MEMS. Differential transformation method (DTM) was used by Ozdemir Ozgumus and Kaya (2010) to study the Flexural–torsional, and free vibration and of a rotating, tapered Timoshenko beam that undergoes flapwise bending vibration. Yaghoobi et al. (2014) calculates the analytical solutions for the post-buckling and nonlinear free vibration analysis of functionally graded (FG) beams resting on nonlinear elastic foundation under thermo-mechanical loadings by using variational iteration method (VIM). Akbari et al. (2017) used a combination of the separation, and Akbari–Ganji's method (AGM) to develop effective solutions for the nonlinear differential equation regulating the nonlinear vibration in arched beams for bridge construction. All these methods have their potential, significant applications, and limitations whereas, metaheuristic techniques based on artificial intelligence are yet to be exploited in this domain.

Recently, intelligent neuro-heuristic techniques based on the approximating ability of artificial neural networks (ANN) are developed to study the solutions for various real problems originating in different fields of engineering and applied sciences, such as the chaotic behavior of wireless communications (Khan et al., 2022a), large deformation in a cantilever beam (Cui et al., 2021), beam–column designs by varying axial loads (Huang et al., 2021), and fluid flow models (Khan et al., 2021b, 2024). The applications of these meta-heuristic techniques are the motivational factors for the authors to exploit the strength of feedforward artificial neural networks with optimization algorithms. The following are some notable features of the presented study:

- The mathematical models for cantilever and double cantilever NEMS actuators with the influence of Van der Waals, Casimir forces, and geometric nonlinearity are formulated and analyzed by developing a soft computing technique based on ANNs and hybridization of optimization techniques such as arithmetic optimization and active set algorithm.
- The designed ANN-AOA-AS algorithm is applied to examine the changes in different physical parameters (applied voltage, Van der Waals, Casimir forces, and axial strains) on the tip and deflection in the beam. The outputs of the proposed scheme are compared with the optimal perturbation iteration method (OPIM), and Runge–Kutta method.
- Statistical, computational, and error analysis in the proposed algorithm's approximate solution are calculated in terms of mean square error (MSE), mean absolute deviations (MAD), root mean square error (RMSE), Nash–Sutcliffe efficiency (NSE) and Error in Nash–Sutcliffe efficiency (ENSE) to study the efficiency, accuracy, and stability of the designed algorithm.

Table 1
Values of various physical parameters involve in the governing mathematical model of the nano-beam.

Parameter	Value
Permittivity of vacuum	8.854×10^{-12} $c^2/\text{N m}^2$
Planck's constant	1.055×10^{-34} J s
Speed of light	2.2998×10^{8} m s^{-1}

2. Governing equation

2.1. Initial model with electrostatic and intermolecular forces

The schematic diagrams of the cantilever and doubly-supported actuators are shown in Figs. 1(a) and 1(b), respectively. Previously, the molecular dynamics (MD) technique was used to investigate the nanostructures. However, this approach is time-demanding and cannot be employed in complicated systems consisting of a large number of atoms. The use of nano-scale continuum models provides an alternative reliable method for simulating the instability of nano-structures. In this study, the continuum nano-scale models are used to describe the nanostructures of actuators. The nano-actuators are modeled by the beam of width (w), length (L), and thickness (h) the initial gap (g) between the ground and a movable beam. The nonlinear differential equation for the actuator's static deflection can be stated using the Euler–Bernoulli beam assumptions as (Abadyan et al., 2010)

$$\tilde{E}I\frac{d^4Y}{dX^4} = f_{elec} + f_k, \quad k = 3,4 \tag{1}$$

here, X denotes the position of the beam along its length as measured from the clamped end, Y is the deflection, and I shows the moment of inertia of the cross-section of the actuator. The effective modulus is $\tilde{E}$ which becomes Young's modulus E for narrow beams when ($w < 5h$) and plate modulus $\frac{E}{1-\upsilon^2}$, where υ is Poisson ratio (Timoshenko et al., 1959). The electrostatic and intermolecular forces per unit length of the beam are f_{elec} and f_k respectively. The electrostatic force per unit length of the actuator is defined using the first-order fringing field correction as

$$f_{\text{elec}} = \frac{\varepsilon_0 w V^2}{2(g-Y)^2}\left(1 + 0.65\frac{(g-Y)}{w}\right), \tag{2}$$

where, V is the applied external voltage, and ε_0 is the permittivity of vacuum. The Van der Waals ($k = 3$), and the Casimir forces ($k = 4$) per unit length of the beam are defined as follows,

$$f_3 = \frac{Aw}{6\pi(g-Y)^3}, \tag{3}$$

$$f_4 = \frac{\pi^2 hcw}{240(g-Y)^4}, \tag{4}$$

here, h is Planck's constant, A is Hamaker constant, and c is the speed of light whose values are dictated in Table 1.

Using Eqs. (2)–(4) in Eq. (1) and defining dimensionless variables $y = \frac{Y}{g}$ and $x = \frac{X}{L}$ will results in the following nonlinear differential equation as

$$\frac{d^4y}{dx^4} - 0.65\frac{g}{w}\frac{\beta}{(1-y(x))} - \frac{\beta}{(1-y(x))^2} = \frac{\alpha_k}{(1-y(x))^k}, \quad k = 3,4, \tag{5}$$

subjected to boundary conditions

$$y = y' = 0 \quad \text{at} \quad x = 0, \quad \text{and} \quad y'' = y''' = 0, \quad \text{at} \quad x = 1 \quad \text{for cantilever beam} \tag{6}$$

$$y = y' = 0 \quad \text{at} \quad x = 0, \quad \text{and} \quad y = y' = 0 \quad \text{at} \quad x = 1 \quad \text{for doubly-supported beam} . \tag{7}$$

where α_k and β correspond to the values of dispersion force and applied voltage which are given as

$$\alpha_k = \begin{cases} \frac{L^4 Aw}{6\pi\tilde{E}Ig^4}, & \text{for Van der Waals interaction } (k=3), \\ \frac{\pi^2 L^4 hcw}{240\tilde{E}Ig^5}, & \text{for Casimir interaction } (k=4), \end{cases} \tag{8}$$

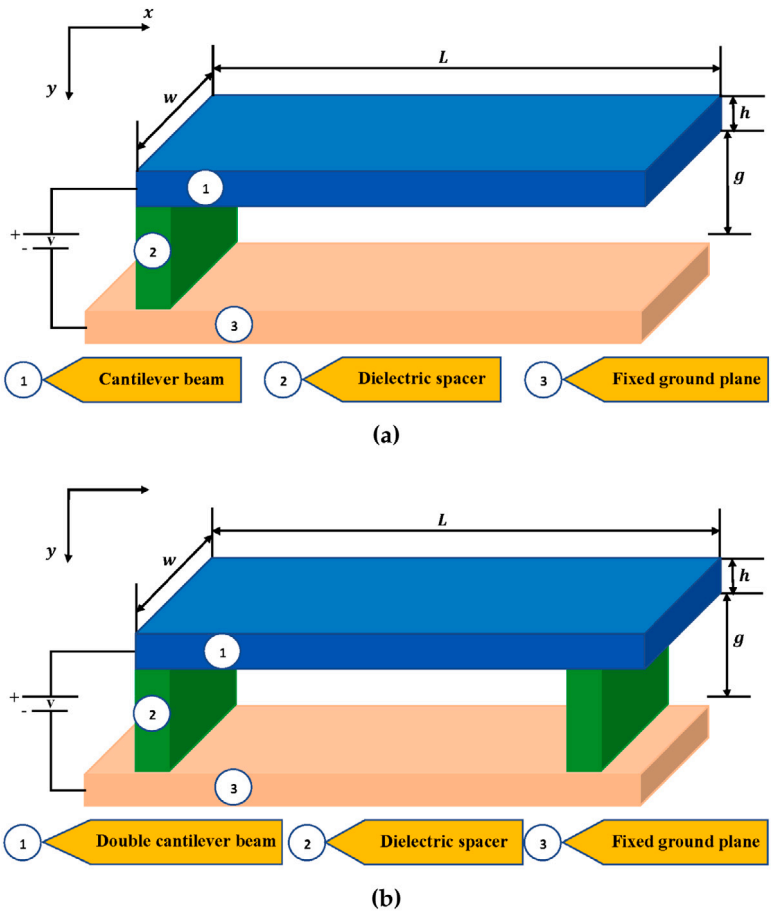

Fig. 1. (a) Schematically depicts the representation of a cantilever and (b) double cantilever nano-beam actuator.

$$\beta = \frac{L^4 \epsilon_0 w V^2}{2\tilde{E} I g^3}. \tag{9}$$

2.2. Geometric nonlinearity using the Kármán model

In the study of microbeams subjected to electric actuation, it is essential to study the geometric nonlinearity to accurately predict the beam's behavior under large deflections. Both bending strain and nonlinear mid-plane stretching strain are included in the total strain in the beam for high deflections. The Kármán model is used to incorporate geometric nonlinearity into the governed equations Eq. (5), as it takes the quadratic component of the second derivative of the deflection. This inclusion accounts for the significant influence of the axial force N from in-plane stretching on beam deflection that can be is given by:

$$N = EA\left(\frac{1}{2}\left(\frac{dY}{dX}\right)^2 - \epsilon_0\right). \tag{10}$$

As a result, the governing differential equation including the geometric nonlinearity term can be expressed as:

$$EI\frac{d^4Y}{dX^4} - N\frac{d^2Y}{dX^2} = f_{\text{elec}} + f_k, \quad k = 3, 4 \tag{11}$$

substituting Eq. (10) in Eq. (11), we get:

$$EI\frac{d^4Y}{dX^4} - EA\left(\frac{1}{2}\left(\frac{dY}{dX}\right)^2 - \epsilon_0\right)\frac{d^2Y}{dX^2} = f_{\text{elec}} + f_k. \tag{12}$$

Again using dimensionless variables $y = \frac{Y}{g}$ and $x = \frac{X}{L}$, we get the following equation:

$$\frac{d^4y}{dx^4} - \lambda\left(\frac{1}{2}\left(\frac{dy}{dx}\right)^2 - \epsilon_0\right)\frac{d^2y}{dx^2} = \frac{\beta}{(1-y(x))^2} + \frac{0.65\beta}{w(1-y(x))} + \frac{\alpha_k}{(1-y(x))^3} + \frac{\alpha_k}{(1-y(x))^4}. \tag{13}$$

where $\lambda = \frac{EA}{EI}$ is a dimensionless parameter representing the relative importance of axial force to bending stiffness.

3. Proposed methodology

In this section, the structure of the proposed ANN-AOA-AS algorithm is presented for calculating the approximate numerical solutions for the governing nonlinear mathematical models Eqs. (5) and (12). The architecture of the design algorithm is divided into two phases. Initially, ANN-based modeling of the problem is performed to construct an unsupervised fitness/objective function with a log-sigmoid activation function. In the second phase, the neurons in ANN architecture are optimized by defining a learning procedure based on hybridization of optimization techniques such as arithmetic optimization and active set algorithm, modeling the global and local search strategies. A schematic workflow of the proposed algorithm is shown in Fig. 2.

3.1. ANN modeling

In many practical applications of applied sciences, artificial neural networks have been widely utilized for modeling and solving nonlinear problems such as temperature distribution in heat exchangers (Khan et al., 2021c), non-Newtonian fluid with heat and mass transfer through

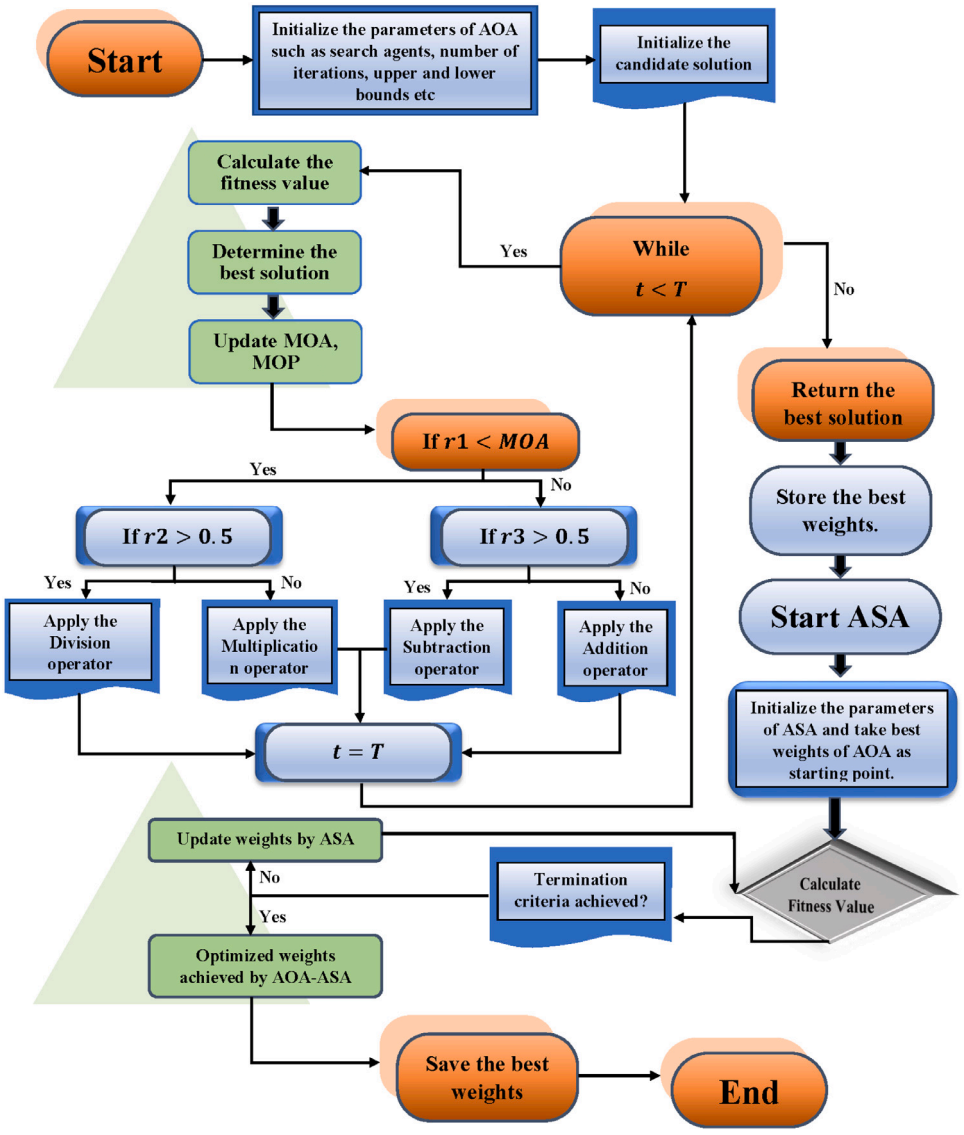

Fig. 2. Working mechanism of the proposed technique.

a porous medium in channel (Khan et al., 2022b), and absorption of carbon dioxide (Khan et al., 2021d,a). The ANN modeling of Eqs. (5) and (12) with boundary conditions is constructed in the form of continuous mapping, the general solution $\hat{y}(x)$ can be defined as:

$$\hat{y}(x) = \sum_{i=1}^{k} \tilde{\chi}_i f\left(\tilde{\zeta}_i x + \tilde{\eta}_i\right), \tag{14}$$

since, $\hat{y}(x)$ is a continuous function so its first, second and nth derivatives are given as

$$\frac{\mathrm{d}\hat{y}}{\mathrm{d}x} = \sum_{i=1}^{k} \tilde{\chi}_i \frac{\mathrm{d}}{\mathrm{d}x} f\left(\tilde{\zeta}_i x + \tilde{\eta}_i\right), \tag{15}$$

$$\frac{\mathrm{d}^2\hat{y}}{\mathrm{d}x^2} = \sum_{i=1}^{k} \tilde{\chi}_i \frac{\mathrm{d}^2}{\mathrm{d}x^2} f\left(\tilde{\zeta}_i x + \tilde{\eta}_i\right), \tag{16}$$

$$\vdots$$

$$\frac{\mathrm{d}^n\hat{y}}{\mathrm{d}x^n} = \sum_{i=1}^{k} \tilde{\chi}_i \frac{\mathrm{d}^n}{\mathrm{d}x^n} f\left(\tilde{\zeta}_i x + \tilde{\eta}_i\right), \tag{17}$$

where, $\tilde{\chi} = \left[\tilde{\chi}_1, \tilde{\chi}_2, \tilde{\chi}_3, \ldots, \tilde{\chi}_k\right], \tilde{\zeta} = \left[\tilde{\zeta}_1, \tilde{\zeta}_2, \tilde{\zeta}_3, \ldots, \tilde{\zeta}_k\right]$ and $\tilde{\eta} = \left[\tilde{\eta}_1, \tilde{\eta}_2, \tilde{\eta}_3, \ldots, \tilde{\eta}_k\right]$ are the adaptive parameters of the neural network, k is the number of neurons and f is the activation function. In this study, log-sigmoid $f(\tau) = 1/(1+e^{-\tau})$ for $\tau = \tilde{\zeta}_i x + \tilde{\eta}_i$, is used as an activation/transfer function. The set of Eqs. (9)–(17) can be expressed as

$$\hat{y}(x) = \sum_{i=1}^{k} \frac{\tilde{\chi}_i}{1 + e^{-(\tilde{\zeta}_i x + \tilde{\eta}_i)}}, \tag{18}$$

$$\frac{\mathrm{d}\hat{y}}{\mathrm{d}x} = \sum_{i=1}^{k} \frac{\tilde{\chi}_i \tilde{\zeta}_i e^{-(\tilde{\zeta}_i x + \tilde{\eta}_i)}}{\left(1 + e^{-(\tilde{\zeta}_i x + \tilde{\eta}_i)}\right)^2}, \tag{19}$$

$$\frac{\mathrm{d}^2\hat{y}}{\mathrm{d}x^2} = \sum_{i=1}^{k} \tilde{\chi}_i \tilde{\zeta}_i^2 \left[\frac{2e^{-2(\tilde{\zeta}_i x + \tilde{\eta}_i)}}{\left(1 + e^{-(\tilde{\zeta}_i x + \tilde{\eta}_i)}\right)^3} - \frac{e^{-(\tilde{\zeta}_i x + \tilde{\eta}_i)}}{\left(1 + e^{-(\tilde{\zeta}_i x + \tilde{\eta}_i)}\right)^2}\right], \tag{20}$$

$$\vdots$$

$$\frac{\mathrm{d}^n\hat{y}}{\mathrm{d}x^n} = \sum_{i=1}^{k} \tilde{\chi}_i \tilde{\zeta}_i^n \left[\begin{array}{l} \frac{n! e^{-n(\tilde{\zeta}_i x + \tilde{\eta}_i)}}{\left(1 + e^{-(\tilde{\zeta}_i x + \tilde{\eta}_i)}\right)^{n+1}} - \frac{n(n-1) e^{-(n-1)(\tilde{\zeta}_i x + \tilde{\eta}_i)}}{\left(1 + e^{-(\tilde{\zeta}_i x + \tilde{\eta}_i)}\right)^{n}} \\ + \frac{n(n-1)(n-2) e^{-(n-2)(\tilde{\zeta}_i x + \tilde{\eta}_i)}}{\left(1 + e^{-(\tilde{\zeta}_i x + \tilde{\eta}_i)}\right)^{n-1}} + \cdots + \frac{(-1)^{n-1} e^{-(\tilde{\zeta}_i x + \tilde{\eta}_i)}}{\left(1 + e^{-(\tilde{\zeta}_i x + \tilde{\eta}_i)}\right)^{2}} \end{array}\right], \tag{21}$$

The appropriate combination of ANN architecture given in Eqs. (16)–(21) are utilized to construct an unsupervised fitness function by

exploitation of approximation theory based on the mean square error (MSE) as

$$\text{Minimize} \quad \zeta = \zeta_1 + \zeta_2, \tag{22}$$

where ζ_1 and ζ_2 correspond to the differential equation and boundary conditions respectively. ζ_1 for governing nonlinear mathematical model of a beam-type nano-electrostatic actuator with electrostatic and intermolecular forces Eq. (5) and geometric nonlinearity model Eq. (12) can be written as:

$$\zeta_1 = \frac{1}{M}\sum_{i=1}^{M}\left(\frac{d^4\hat{y}_i}{dx^4} - \frac{\alpha_k}{(1-\hat{y}_i(x))^k} - \frac{\beta}{(1-\hat{y}_i(x))^2} - 0.65\frac{g}{w}\frac{\beta}{(1-\hat{y}_i(x))}\right)^2, \tag{23}$$

$$\begin{aligned}\zeta_1 = &\frac{1}{M}\sum_{i=1}^{M}\left(\frac{d^4\hat{y}_i}{dx^4} - \lambda\left(\frac{1}{2}\left(\frac{d\hat{y}_i}{dx}\right)^2 - \epsilon_0\right)\frac{d^2\hat{y}_i}{dx^2} - \frac{\beta}{(1-\hat{y}_i(x))^2}\right.\\ &\left. - 0.65\frac{\beta}{w(1-\hat{y}_i(x))} - \frac{\alpha_k}{(1-\hat{y}_i(x))^3} - \frac{\alpha_k}{(1-\hat{y}_i(x))^4}\right)^2.\end{aligned} \tag{24}$$

The boundary conditions are also modeled as follows

$$\zeta_2 = \frac{1}{4}\left((\hat{y}(0)-0)^2 + \left(\hat{y}'(0)-0\right)^2 + \left(\hat{y}''(1)-0\right)^2 + \left(\hat{y}'''(1)-0\right)^2\right), \tag{25}$$

for doubly-supported beam ζ_2 can be written as

$$\zeta_2 = \frac{1}{4}\left((\hat{y}(0)-0)^2 + \left(\hat{y}'(0)-0\right)^2 + (\hat{y}(1)-0)^2 + \left(\hat{y}'(1)-0\right)^2\right). \tag{26}$$

where $\hat{y}_i = \hat{y}\left(x_i\right), x_i = ih, h = 1/M$. For best set of weights in ANN structure the value of ζ approaches to zero that will reflect the overlapping of approximate solution over exact solution.

3.2. Optimization process

In this section, the learning of unknown variables of the ANN architecture is carried out by utilizing the hybridization of metaheuristic techniques such as arithmetic optimization algorithm and local search capability of active set algorithm.

3.2.1. Arithmetic optimization algorithm

The arithmetic optimization algorithm (AOA) is a novel meta-heuristic algorithm presented by Abualigah et al. (2021) in 2021. This algorithm's fundamental idea is to integrate the four standard arithmetic operators in mathematics, namely division (D), multiplication (M), addition (A), and subtraction (S). The AOA replicates the distribution features of the four fundamental arithmetic operations, and, like other meta-heuristic algorithms, it divides the search process into two distinct phases: exploration and exploitation. The exploration phase updates the positions of candidates (solutions) using multiplication and division operators, whereas the exploitation phase incorporates addition and subtraction operations. Fig. 3 depicts the order of Arithmetic operators and their dominance as they progress from the outside to the interior of the circle.

The AOA initializes the process by randomly generating an individual (candidate solution) X from the global search space (population space) as shown in Eq. (27).

$$X = \begin{bmatrix} x_{1,1} & \cdots & \cdots & x_{1,j} & x_{1,n-1} & x_{1,n} \\ x_{2,1} & \cdots & \cdots & x_{2,j} & \cdots & x_{2,n} \\ \cdots & \cdots & \cdots & \cdots & \cdots & \cdots \\ \vdots & \vdots & \vdots & \vdots & \vdots & \vdots \\ x_{N-1,1} & \cdots & \cdots & x_{N-1,j} & \cdots & x_{N-1,n} \\ x_{N,1} & \cdots & \cdots & x_{N,j} & x_{N,n-1} & x_{N,n} \end{bmatrix}, \tag{27}$$

where N denotes the number of individual solutions in the population space, the number of design variables is denoted by n, and $x_{i,j}$ shows the jth component of i candidate solution in the initial population. Afterward, an AOA uses a dynamic function called Math Optimizer Accelerated (MOA) to identify the search space for exploration and exploitation during the process. The MOA function's is defined as follows:

$$\text{MOA}\left(C_{Iter}\right) = \text{Min} + C_{Iter} \times \left(\frac{Max - Min}{M_{Iter}}\right), \tag{28}$$

here, C_{Iter} denotes the current iteration that lies between 1 and maximum iteration, Max, and Min are the maximum and minimum values of the dynamical accelerated function. If $r1 > MOA$, the function MOA is used to activate the exploration phase, where r1 is a random value. Since Multiplication (M) and Division (D) are two operators that easily accomplish with high dissipation, therefore these operators are used for the exploitation stage. Fig. 4 depicts the methodology of updating the position of an individual by AOA based on the operators in the search space. The mathematical behavior of the exploitation phase is given as

$$x_{i,j}\left(C_{Iter}+1\right) = \begin{cases} best\left(x_j\right) \div (MOP + \epsilon) \times \left(\left(UB_j - LB_j\right) \times \mu + LB_j\right), \\ r2 < 0.5 \\ best\left(x_j\right) \times MOP \times \left(\left(UB_j - LB_j\right) \times \mu + LB_j\right), \\ \text{otherwise} \end{cases} \tag{29}$$

where, $x_{i,j}\left(C_{Iter}+1\right)$ is a newly generated position, UB_j and LB_j are the upper and lower bounds for the jth design variables, $best\left(x_j\right)$ is the best candidate found at the ith iteration, ϵ is a very small plosive number, and μ is controlling coefficient (0.4999) (Abualigah et al., 2021). Moreover, MOP is a constant coefficient which is defined as

$$MOP\left(C_{Iter}\right) = 1 - \frac{{C_{Iter}}^{1/\alpha}}{{M_{Iter}}^{1/\alpha}}, \tag{30}$$

here, α is a sensitive parameter that determines the precision of exploitation over the course of an iteration. Furthermore, an exploitation search is adopted to calculate the near optimum by using Addition (A) and Subtraction (S).

$$x_{i,j}\left(C_{Iter}+1\right) = \begin{cases} best\left(x_j\right) - MOP \times \left(\left(UB_j - LB_j\right) \times \mu + LB_j\right), \\ r3 < 0.5 \\ best\left(x_j\right) + MOP \times \left(\left(UB_j - LB_j\right) \times \mu + LB_j\right), \\ \text{otherwise} \end{cases} \tag{31}$$

Fig. 4 demonstrates how a search solution adjusts its positions in a two-dimensional search space according to arithmetic operators. In exploitation, the first operator (S) is conditioned by $r3 < 0.5$ and the other operator (A) will be neglected until this operator finishes its current task.

In both phases, it is observed that the fitness value of the objective function will correspond to the value of ith candidate solution and will be replaced with the current solution when the fitness value is improved.

3.2.2. The proposed ANN-AOA-AS algorithm

Metaheuristic algorithms (MA) are high-level techniques or heuristics that are designed to find, generate, or provide a sufficiently good solution to optimization problems arising in various domains of applied physics and mathematics. AOA is a metaheuristic algorithm and has the weaknesses of insufficient exploration capability and is likely to fall into local optima. Therefore, to overcome this draw back ANN-AOA is hybridized with the active set (AS) algorithm to improve the local search convergence of the proposed technique. AS algorithm is an efficient technique proposed in Hristov and Fallone (1997) to solve complex optimization problems. Recently, AS algorithm has been used to solve the second-order conic-constrained quadratic programming (Goldberg and Leyffer, 2015), transportation discrete network design bi-level

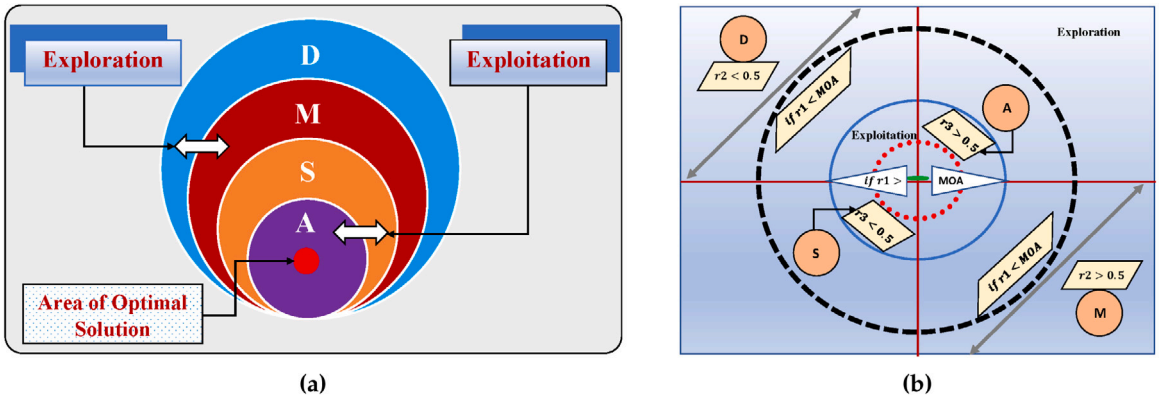

Fig. 3. (a) depicts the AOA's hierarchy of operators (supremacy decreases from top to bottom) and (b) illustrates the AOA's search phases.

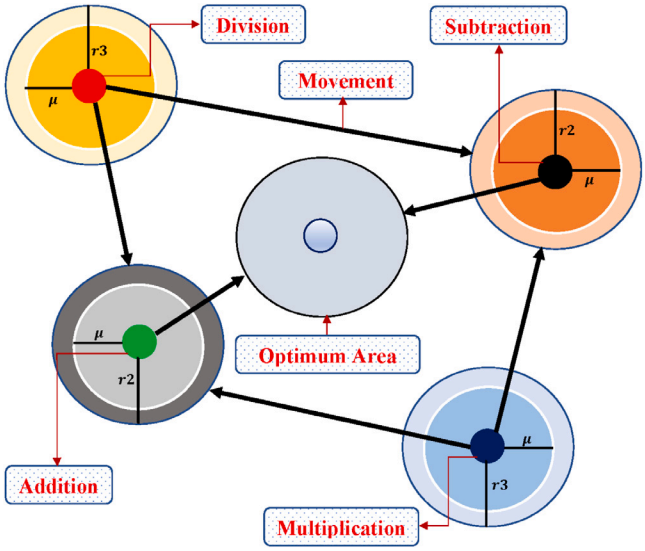

Fig. 4. Model for repositioning math operators in AOA in the direction of the optimum solution.

problem (Wang and Pardalos, 2017), feasibility restoration in power systems (Phan and Ghosh, 2016), and stability torque allocation of distributed drive electric vehicles (Zhang et al., 2017). The pseudo-code of the proposed algorithm is shown in Table 2.

4. Result and discussion

In this section, the experimental setup and detailed discussions are demonstrated, based on the implementation of the proposed ANN-AOA-AS algorithm for different variations in physical parameters on cantilever and double-supported beams. To study the dynamics of the nanoelectromechanical systems (NEMS) following scenarios are considered.

Scenario 1: In this scenario Eqs. (5)–(7) are considered to study the influence of applied voltage, dispersion forces, Van der Waals and Casimir forces on the deflection of the cantilever and double supported beam.

Scenario 2: In this scenario, a special case of nanoelectromechanical systems (NEMS) is considered when the separation between the particles is less than 20 nm. The forces between the two surfaces (ground and the beam) are named as quantum Casimir forces (Rodriguez et al., 2011; Abdi et al., 2011) and the mathematical model for such case is given as (Adel and Deniz; Fazli et al., 2014)

$$\frac{d^4y}{dx^4} = \frac{\alpha_k}{(1-y(x))^k} + \frac{\beta}{(1-y(x))^2} + \frac{\gamma}{(1-y(x))} \tag{32}$$

with boundary conditions

$$y = y' = 0 \quad \text{at} \quad x = 0, \quad \text{and} \quad y'' = y''' = 0, \quad \text{at} \quad x = 1. \tag{33}$$

Scenario 3: we consider the governing nonlinear mathematical model of a Beam-Type Nano-Electrostatic actuator with geometric nonlinearity Eq. (12) to study the combined effects of different parameters on the deflection of both cantilever and doubly-supported beams.

Furthermore, a novel integrated soft computing approach is developed and implemented to optimize the fitness functions for scenario 1 and 2 to study the different cases of Eqs. (5)–(9) and Eqs. (32)–(33) respectively. Fig. 5 shows the effect of variations in applied voltage between the ground surface and the beam under Van der Waals and Casimir forces $\alpha_k = 0.5$ with $\gamma = 0.2$ and $g/w = 1$. It is observed that the deflection of a typical nano-beam actuator increases with an increase in β. Also, the intensity of deflection in the doubly supported beam is negligible as compared to the cantilever beam. The statistics of the approximate solutions and absolute errors calculated by the designed ANN-AOA-AS paradigm for different values of applied voltage in scenarios 1 and 2 are dictated in Tables 3–5. Fig. 6 shows the absolute errors (AE's) in cases of scenarios 1 and 2 that lie between 10^{-4} to 10^{-7}, reflecting the perfect overlapping of approximate solutions over the exact. The accuracy and novelty of the proposed paradigm are deduced from the comparison of the absolute errors with optimal perturbation iteration method (OPIM) (Adel and Deniz) as shown in Tables 6 and 7 respectively.

The graphical analysis on the tip of the beam $(y(1))$ under the influence of variations in applied voltage, γ, Van der Waals, and Casimir forces are depicted in Fig. 7. The plot of β versus g/w presented in Fig. 7(a) shows that increasing applied voltage and values of g/w will cause an increase in the deflection of the caviler beam. The analysis illustrates that the intensity deflection by the Van der Waals forces is much higher than the Casimir forces. It is noticed that even without an applied voltage when the distance between the cantilever beam and the ground plane is small enough, the beam can collapse into the ground plane due to intermolecular forces (Zare et al., 2017).

Lastly, we consider scenario 3 and explore the combined effects of geometric nonlinearity parameter λ and initial axial strain ϵ_0. The contour plots generated for the cantilever and doubly-supported beams provide valuable insights into the deflection behavior. Fig. 8(a) for the cantilever beam shows the deflection $y(x)$ at $x = 1$. It reveals that as λ increases, the deflection generally increases due to the enhanced geometric nonlinearity, which intensifies the beam's response to applied forces. Similarly, higher values of ϵ_0 lead to greater deflection, reflecting the additional pre-stress in the beam. The combined effect of high λ and ϵ_0 values results in significantly amplified deflections, indicating a synergistic interaction between these parameters. This finding underscores the importance of accounting for both geometric nonlinearity and initial axial strain in the analysis and design of beams, especially in advanced applications like MEMS and nanoscale devices,

Table 2
Pseudo code of proposed hybrid soft computing technique ANN-AOA-IPA.

Global Search Phase
Arithmetic Optimization Algorithm : Start
Step 1: Initialization: AOA Randomly generates an initial population, with parameters equal in number to the neurons in ANN architecture.
W=[$\tilde{\chi}$, $\tilde{\varsigma}$, $\tilde{\eta}$]
where, $\tilde{\chi} = [\tilde{\chi}_1, \tilde{\chi}_2, \tilde{\chi}_3, \ldots, \tilde{\chi}_k]$, $\tilde{\varsigma} = [\tilde{\varsigma}_1, \tilde{\varsigma}_2, \tilde{\varsigma}_3, \ldots, \tilde{\varsigma}_k]$, $\tilde{\eta} = [\tilde{\eta}_1, \tilde{\eta}_2, \tilde{\eta}_3, \ldots, \tilde{\eta}_k]$
Step 2: Fitness Calculation: Calculate the fitness/ Objective value of each W by using Eq. (22), and within the search zone, a random solution is generated.
Step 3: Termination criteria : Stop AOA if the following criteria for termination is achieved.
- Reached pre-defined number of iterations.
- Fitness $\leq 10^{-20}$
- Function Tolerance $\leq 10^{-18}$

Step 4: Storage : Saves the best set of weights such as $W_{best-AOA}$.
Arithmetic optimization algorithm : End
Local Search Phase
Active Set Algorithm: Start
Step 5: Initialization: AS algorithm initializes the process by exploiting the search space around the set of weights obtained by AOA i.e. $W_{best-AOA}$.
Step 6: Fitness Calculation: The fitness value is calculated for the set of updated weights. ASA tune the weights in ANN stricture for minimization of the objective function.
Step 7: Termination criteria : ASA continues the process until the following termination criteria is achieved.
- Reached pre-defined number of iterations i.e 1000.
- Fitness $\leq 10^{-20}$
- Function Tolerance $\leq 10^{-15}$

Step 4: Storage : Saves the best set of updated weights such as $W_{best-AOA-ASA}$.
Active Set Algorithm: End

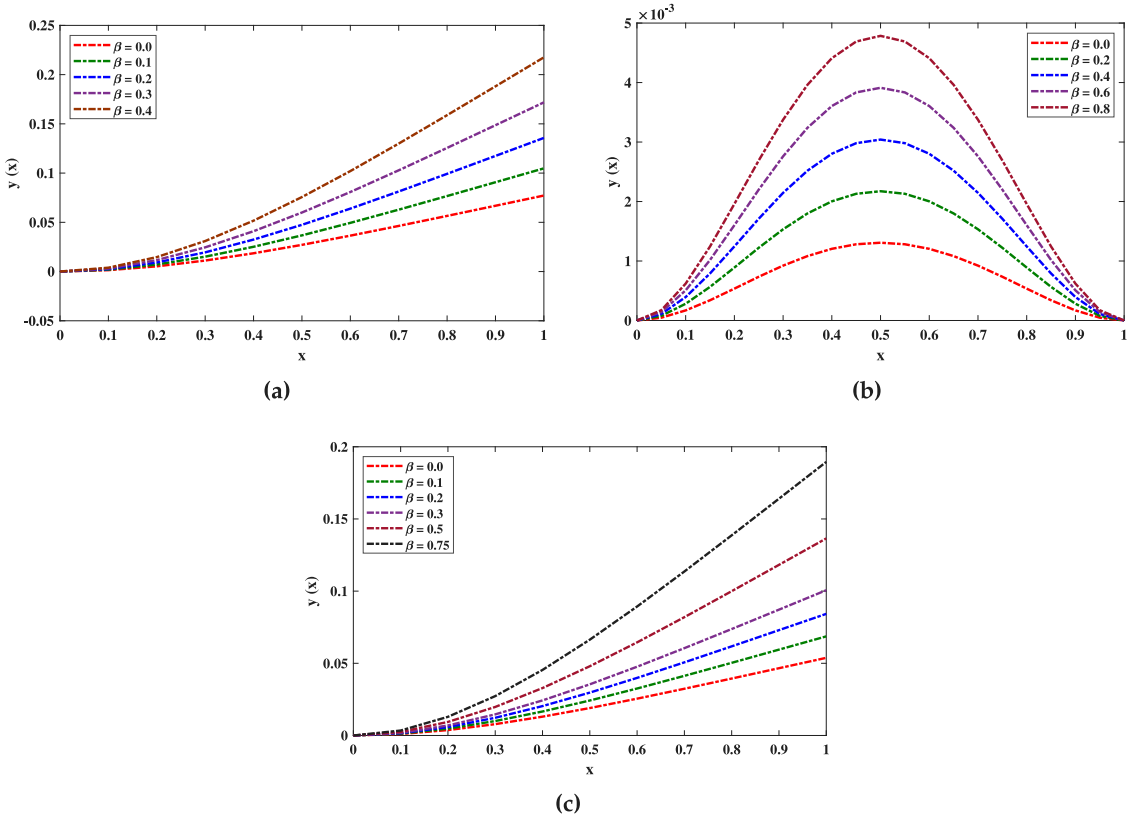

Fig. 5. (a)–(c) shows the effect of changes in applied voltage on the deflection of the cantilever and doubly supported beam.

where these factors can critically influence performance and reliability. Fig. 8(b) for the doubly-supported beam shows the deflection $y(x)$ at $x = 0.5$. It similarly illustrates that higher λ and ϵ_0 values lead to increased deflections. The combined effects are evident in both beam types, with the doubly-supported beam showing a different distribution of deflection due to the different boundary conditions. These analyses reveal the significant impact of geometric nonlinearity, and initial axial strain on beam deflection, highlighting the necessity of incorporating these factors into design considerations for precise control and optimization in advanced engineering applications. The results for the cantilever beam under varying β, λ, and ϵ_0 values provide comprehensive insights into the underlying mechanics and emphasize the need for detailed modeling in the design of flexible beam structures.

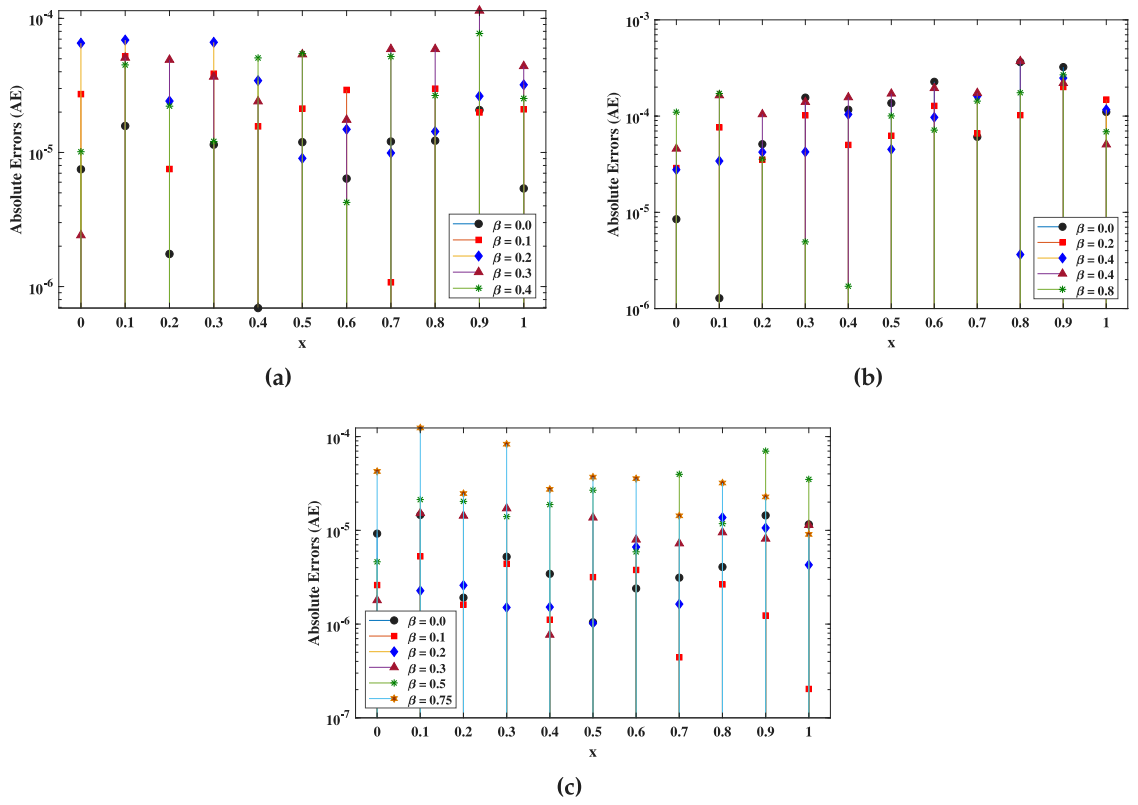

Fig. 6. (a)–(c) shows the absolute errors in the solutions for varying applied voltage in scenarios 1 and 2.

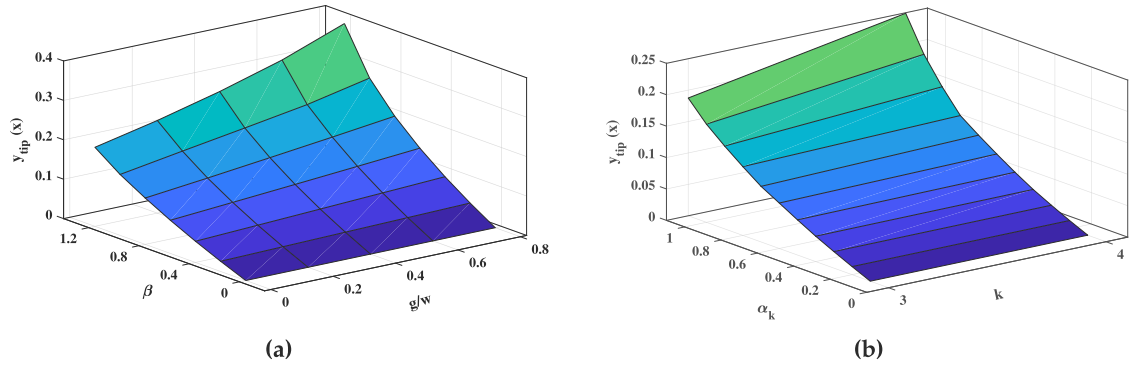

Fig. 7. (a)–(b) shows the effect of different forces along with variations in applied voltage on the tip of a cantilever beam.

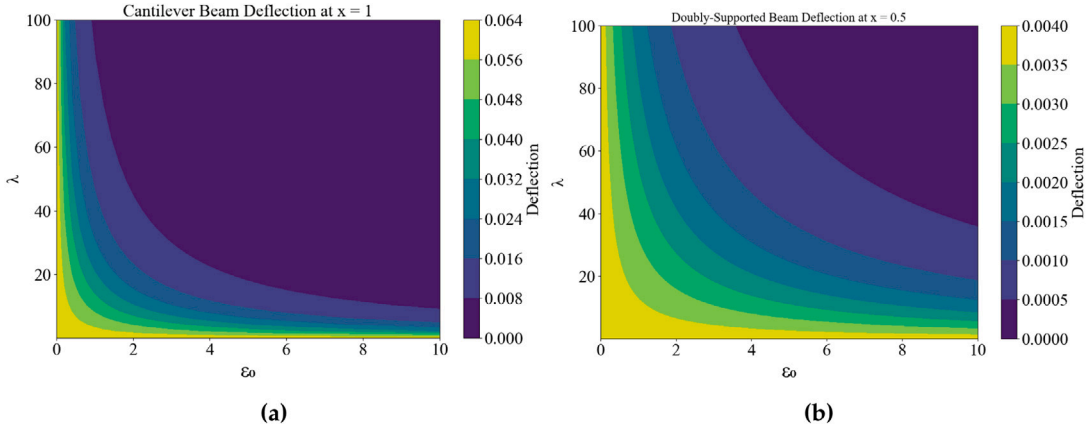

Fig. 8. (a)–(b) Contour plots showing the deflection behavior of both cantilever and doubly-supported beams.

Table 3
Statistics of approximate solutions obtained by the designed paradigm for various cases of Doubly supported, and cantilever beam.

	Cantilever Beam					Doubly Supported Beam				
	$\beta = 0.0$	$\beta = 0.1$	$\beta = 0.2$	$\beta = 0.3$	$\beta = 0.4$	$\beta = 0.0$	$\beta = 0.2$	$\beta = 0.4$	$\beta = 0.6$	$\beta = 0.8$
0.0	7.87522E−07	−3.47147E−06	−1.25643E−05	−2.10474E−05	2.66257E−05	8.48690E−06	2.88653E−05	2.77423E−05	4.58056E−05	1.09843E−04
0.1	0.001414612	0.001908311	0.002448214	0.003078336	0.003915621	0.000169394	0.000281536	0.000393958	0.000506663	0.000619655
0.2	0.005301512	0.007168334	0.009231957	0.011628662	0.014666377	0.000535409	0.000889922	0.001245354	0.001601713	0.001959004
0.3	0.011166837	0.015113253	0.019491749	0.024576672	0.030978176	0.000922415	0.001533233	0.002145676	0.002759757	0.003375488
0.4	0.018567082	0.025146478	0.032463193	0.040967609	0.051665184	0.001204861	0.002002757	0.002802812	0.003605040	0.004409457
0.5	0.027111104	0.036740055	0.047467125	0.059949074	0.075661851	0.001307385	0.002173192	0.003041354	0.003911887	0.004784810
0.6	0.036461706	0.049437137	0.063913270	0.080776267	0.102030349	0.001204858	0.002002754	0.002802809	0.003605037	0.004409454
0.7	0.046337547	0.062855001	0.081304770	0.102818555	0.129970162	0.000922410	0.001533227	0.002145671	0.002759752	0.003375482
0.8	0.056515332	0.076688558	0.099243528	0.125567396	0.158829962	0.000535402	0.000889915	0.001245347	0.001601706	0.001958997
0.9	0.066832253	0.090714337	0.117436349	0.148645630	0.188121994	0.000169381	0.000281525	0.000393948	0.000506655	0.000619646
1.0	0.077188638	0.104794884	0.135701871	0.171818251	0.217539204	−8.48434E−07	−4.65825E−06	−4.48004E−07	−5.64151E−07	−4.46935E−08

Table 4
Absolute errors in the proposed ANN-AOA-AS algorithm's approximate solutions for changes in applied voltage in scenario 1.

	Cantilever Beam					Doubly Supported Beam				
	$\beta = 0.0$	$\beta = 0.1$	$\beta = 0.2$	$\beta = 0.3$	$\beta = 0.4$	$\beta = 0.0$	$\beta = 0.2$	$\beta = 0.4$	$\beta = 0.6$	$\beta = 0.8$
0.0	7.4899E−06	2.7240E−05	6.5385E−05	2.4113E−06	1.0127E−05	8.4869E−06	2.8865E−05	2.7742E−05	4.5804E−05	1.0984E−04
0.1	1.5763E−05	5.2165E−05	6.8942E−05	5.0872E−05	4.4936E−05	1.2820E−06	7.6282E−05	3.4132E−05	1.6416E−04	1.7178E−04
0.2	1.7501E−06	7.5261E−06	2.4172E−05	4.9079E−05	2.2164E−05	5.1111E−05	3.5230E−05	4.2251E−05	1.0439E−04	3.5669E−05
0.3	1.1433E−05	3.8650E−05	6.6313E−05	3.6728E−05	1.2079E−05	1.5567E−04	1.0187E−04	4.2442E−05	1.4012E−04	4.9248E−06
0.4	6.9148E−07	1.5658E−05	3.4341E−05	2.4033E−05	5.0666E−05	1.1659E−04	5.0184E−05	1.0416E−04	1.5664E−04	1.7059E−06
0.5	1.1936E−05	2.1232E−05	9.0386E−06	5.3888E−05	5.4561E−05	1.3651E−04	6.2528E−05	4.5137E−05	1.7112E−04	1.0026E−04
0.6	6.3839E−06	2.9258E−05	1.4879E−05	1.7516E−05	4.2409E−06	2.2728E−04	1.2769E−04	9.7041E−05	1.9507E−04	7.1522E−05
0.7	1.2065E−05	1.0759E−06	9.9110E−06	5.9006E−05	5.1907E−05	6.0816E−05	6.5980E−05	1.6104E−04	1.7384E−04	1.4328E−04
0.8	1.2237E−05	2.9893E−05	1.4322E−05	5.8998E−05	2.6600E−05	3.6372E−04	1.0226E−04	3.6447E−06	3.7213E−04	1.7481E−04
0.9	2.0715E−05	1.9882E−05	2.6307E−05	1.1412E−04	7.7127E−05	3.2307E−04	2.0042E−04	2.4868E−04	2.2012E−04	2.6796E−04
1.0	5.3908E−06	2.0998E−05	3.1960E−05	4.4038E−05	2.5257E−05	1.1035E−04	1.4857E−04	1.1661E−04	5.0654E−05	6.8686E−05

Table 5
Results of approximate solutions and absolute errors for different values β in scenario 2.

	Approximate Solutions						Absolute Errors					
	$\beta = 0.0$	$\beta = 0.1$	$\beta = 0.2$	$\beta = 0.3$	$\beta = 0.5$	$\beta = 0.75$	$\beta = 0.0$	$\beta = 0.1$	$\beta = 0.2$	$\beta = 0.3$	$\beta = 0.5$	$\beta = 0.75$
0.0	−3.11756E−07	−2.05E−07	−2.20E−07	1.89E−07	−3.66E−06	−1.92E−05	9.2268E−06	2.6078E−06	7.1472E−07	1.7959E−06	4.6181E−06	4.2477E−05
0.1	9.98146E−04	0.001271552	0.001556796	0.00185552	0.002500386	0.003430587	1.4588E−05	5.2797E−06	2.2709E−06	1.5250E−05	2.1294E−05	1.2361E−04
0.2	3.73478E−03	0.004758861	0.005828405	0.00694915	0.009381782	0.012926143	1.9134E−06	1.6125E−06	2.5921E−06	1.4307E−05	2.0348E−05	2.4675E−05
0.3	7.85141E−03	0.010007277	0.012260531	0.01462358	0.019762118	0.027275958	5.2294E−06	4.3907E−06	1.5040E−06	1.7139E−05	1.4009E−05	8.2957E−05
0.4	1.30302E−02	0.016612863	0.020359851	0.024292354	0.032854812	0.045406822	3.4337E−06	1.1144E−06	1.5181E−06	7.6858E−07	1.8844E−05	2.7383E−05
0.5	1.89939E−02	0.024222726	0.029694581	0.035441167	0.047967054	0.066367299	1.0457E−06	3.1684E−06	1.0226E−06	1.3664E−05	2.6803E−05	3.6956E−05
0.6	2.55064E−02	0.032535703	0.03989550	0.047629301	0.064502372	0.089332388	2.3980E−06	3.7795E−06	6.6397E−06	7.9563E−06	5.8952E−06	3.5556E−05
0.7	3.23731E−02	0.041303173	0.050657159	0.060491349	0.081963731	0.113609298	3.1282E−06	4.4222E−07	1.6345E−06	7.2455E−06	3.9600E−05	1.4284E−05
0.8	3.94417E−02	0.050329975	0.061739258	0.073739167	0.099957106	0.138644276	4.0678E−06	2.6511E−06	1.3702E−05	9.5079E−06	1.1775E−05	3.1993E−05
0.9	0.04660252	0.059475395	0.072968151	0.087164031	0.118195491	0.164030477	1.4429E−05	1.2347E−06	1.0613E−05	8.1384E−06	7.0035E−05	2.2740E−05
1.0	0.053789242	0.068654229	0.084238451	0.100638966	0.136503313	0.189516838	1.1575E−05	2.0331E−07	4.2791E−06	1.1393E−05	3.4941E−05	9.0543E−06

Table 6
Comparison of the absolute errors in the ANN-AOA-AS algorithms solution with optimal perturbation iteration method for Casimir forces (K=3) and applied voltage ($\beta = 0.55$).

	$\gamma = 0.2, \alpha = 0.2$		$\gamma = 0.25, \alpha = 0.25$		$\gamma = 0.2, \alpha = 0.3$		$\gamma = 0.3, \alpha = 0.3$	
	OPIM	ANN-AOA-ASA	OPIM	ANN-AOA-ASA	OPIM	ANN-AOA-ASA	OPIM	ANN-AOA-ASA
0.1	8.8733E−04	3.7433E−04	1.9616E−02	2.0034E−04	2.9424E−02	3.1484E−05	3.9232E−01	3.0783E−06
0.2	1.4907E−03	1.9657E−04	4.6314E−03	3.2186E−06	6.9471E−03	1.6937E−05	9.2628E−02	4.2395E−06
0.3	1.7042E−03	2.6893E−04	1.8686E−03	1.3446E−04	2.8029E−03	3.4618E−05	3.7372E−02	2.3926E−05
0.4	1.3982E−03	8.3372E−05	9.1129E−04	9.3490E−05	1.3669E−03	5.7380E−06	1.8226E−02	1.9008E−05
0.5	4.1926E−04	2.8464E−04	4.7638E−04	3.1388E−05	7.1457E−04	4.1015E−05	9.5277E−03	2.6439E−05
0.6	1.4096E−03	6.2102E−05	2.4736E−04	1.1224E−04	3.7105E−04	1.4900E−05	4.9473E−03	3.3697E−05
0.7	4.2888E−03	2.7924E−04	1.1584E−04	9.3697E−05	1.7375E−04	4.3952E−05	2.3167E−03	2.9093E−05
0.8	8.4424E−03	1.7417E−04	3.6569E−05	1.7713E−05	5.4854E−05	3.5597E−05	7.3138E−03	5.7447E−05
0.9	1.4118E−02	3.9117E−04	1.2007E−05	3.7440E−05	1.8011E−05	7.1245E−05	2.4014E−04	4.2928E−05
1.0	2.1585E−02	1.5229E−04	4.1215E−05	1.0812E−05	6.1823E−05	2.7340E−05	8.2430E−04	1.4633E−05

4.1. Performance measures

In this section, different performance measures are defined to assess the efficiency, accuracy, and stability of the designed novel meta-heuristic approach. The results obtained by the proposed ANN-AOA-AS algorithm are analyzed by defining fitness function based on mean square error, Theil's inequality coefficient (TIC), mean absolute deviation (MAD), root mean square error (RMSE), and error in Nash–Sutcliffe efficiency (ENSE). The mathematical formulation of MAD, TIC, RMSE, and ENSE is given as

$$MAD = \frac{1}{M}\sum_{i=1}^{M}\left(\left|\hat{y}\left(x_i\right) - y\left(x_i\right)\right|\right), \tag{34}$$

Table 7
Comparison of the absolute errors in the ANN-AOA-AS algorithms solution with optimal perturbation iteration method for Van der Waals force ($K = 4$) and applied voltage ($\beta = 0.25$).

	$\gamma = 0.2, \alpha = 0.2$		$\gamma = 0.25, \alpha = 0.25$		$\gamma = 0.2, \alpha = 0.3$		$\gamma = 0.3, \alpha = 0.3$	
	OPIM	ANN-AOA-ASA	OPIM	ANN-AOA-ASA	OPIM	ANN-AOA-ASA	OPIM	ANN-AOA-ASA
0.1	1.0570E−07	1.8698E−05	5.2010E−06	5.6762E−05	1.9910E−06	8.2422E−06	1.0440E−06	1.5779E−04
0.2	7.9910E−06	6.4661E−06	9.1110E−06	4.6747E−06	7.7710E−06	6.8734E−05	9.0120E−06	2.4080E−05
0.3	6.8060E−04	1.9892E−05	3.8970E−06	2.0407E−05	1.2710E−05	2.3205E−06	3.2410E−05	1.0048E−04
0.4	1.6130E−03	9.4127E−06	3.9550E−07	5.8437E−05	5.3550E−05	4.0620E−05	1.8210E−04	1.9618E−05
0.5	3.1510E−03	1.0181E−05	2.9470E−03	3.4199E−05	1.6340E−04	2.4296E−05	6.9450E−04	7.0963E−05
0.6	5.4450E−03	1.9587E−05	1.5210E−03	2.2641E−05	4.0660E−04	1.4170E−05	2.0740E−03	4.8206E−05
0.7	8.6460E−03	1.0944E−05	6.0890E−03	5.4977E−05	8.7890E−04	2.2618E−05	5.2290E−03	5.3184E−05
0.8	1.2910E−02	6.2447E−06	2.0250E−02	2.6911E−05	1.7140E−03	1.0557E−05	1.1650E−02	6.2736E−05
0.9	1.8380E−02	1.1937E−05	5.8460E−02	3.4495E−05	3.0880E−03	3.0567E−05	2.3620E−02	9.5599E−05
1.0	2.5210E−02	2.7814E−06	1.5090E−01	8.2538E−06	5.2290E−03	1.0080E−05	4.4450E−02	3.9827E−05

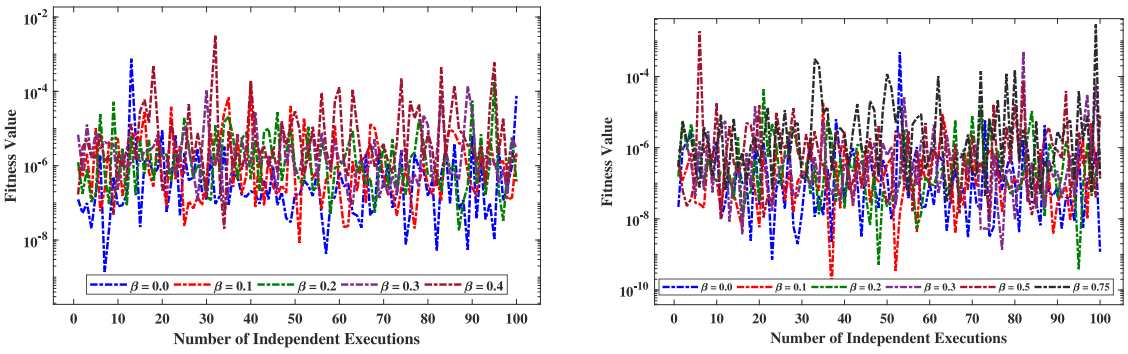

(a) Scenario 1 **(b)** Scenario 2

Fig. 9. The results of unsupervised behavior of the fitness function during the multiple executions of the proposed technique for scenario 1 and 2.

$$TIC = \frac{\sqrt{\frac{1}{M}\sum_{i=1}^{M}\left(\hat{y}\left(x_i\right) - y\left(x_i\right)\right)^2}}{\sqrt{\frac{1}{M}\sum_{i=1}^{M}\left(\hat{y}\left(x_i\right)\right)^2} + \sqrt{\frac{1}{M}\sum_{i=1}^{M}\left(y\left(x_i\right)\right)^2}}, \tag{35}$$

$$RMSE = \sqrt{\frac{1}{M}\sum_{i=1}^{M}\left(\hat{y}\left(x_i\right) - y\left(x_i\right)\right)^2}, \tag{36}$$

$$ENSE = |1 - NSE|, \tag{37}$$

where NSE is Nash–Sutcliffe Efficiency and is defined as

$$NSE = 1 - \left(\frac{\sum_{i=1}^{M}\left(\hat{y}\left(x_i\right) - y\left(x_i\right)\right)^2}{\sum_{i=1}^{M}\left(y\left(x_i\right) - \frac{1}{M}\sum_{i=1}^{M}\left(y\left(x_i\right)\right)\right)^2}\right). \tag{38}$$

here, $\hat{y}$ and y are the approximate and exact solution for the problem. M corresponds to the total number of mesh (grid) points and i denotes the number of current solution points. To investigate the efficiency, stability, and durability of the results, the design method is executed 100 times. The behavior of fitness value in each run is graphically shown through Figs. 9. In addition, the values of MAD and ENSE for the scenario are plotted through Figs. 10 and 11 respectively.

An extensive statistical study is conducted based on performance measures such as minimum, mean, and standard deviations for scenarios 1 and 2 as shown in Table 8. The analysis shows that minimum (Min.) values of each fitness/ objective function, MAD, TIC, RMSE, and ENSE lie in between 10^{-8} to 10^{-11}, 10^{-5} to 10^{-7}, 10^{-5} to 10^{-6}, 10^{-6} to 10^{-7}, and 10^{-7} to 10^{-9} respectively. Additionally, the accuracy of the solutions is also dictated by the mean values of the performance indices that lie around 10^{-5} to 10^{-7}, 10^{-4} to 10^{-5}, 10^{-3} to 10^{-4}, 10^{-3} to 10^{-5} and 10^{-4} to 10^{-5} respectively.

5. Conclusion

In this study, we developed and implemented an integrated soft computing paradigm based on artificial neural networks (ANNs) combined with the arithmetic optimization algorithm (AOA) and active set algorithm (ASA) to analyze the nonlinear mathematical model of beam-type nanoelectrostatic actuators, including cantilevers and doubly-supported beams. The proposed ANN-AOA AS algorithm optimized fitness functions for different scenarios, varying applied voltage, Van der Waals, and Casimir forces to study beam deflection. The results showed that deflection increases with higher applied voltage, and Van der Waals forces induce significantly higher deflection in cantilever beams compared to Casimir forces. The analysis revealed that as geometric nonlinearity parameter λ and initial axial strain ϵ_0 increase, deflection also increases, highlighting the importance of these parameters in beam response.

The statistical analysis comparing the proposed algorithm's approximate solutions with state-of-the art methods showed near-perfect overlap, indicating precise modeling. Performance measures such as MAD, TIC, RMSE, and ENSE validated the stability, accuracy, and efficiency of the ANN-AOA-AS algorithm, with mean percentage values of these indices around 10^{-4} to 10^{-6}. These findings underscore the necessity of incorporating geometric nonlinearity, initial axial strain, and intermolecular forces in designing and optimizing NEMS beam-type actuators to ensure optimal performance and reliability in advanced engineering applications.

Replication of results

Essential details for replication of results have been described in the manuscript. Further, the data and MATLAB codes are made open sources and available upon request.

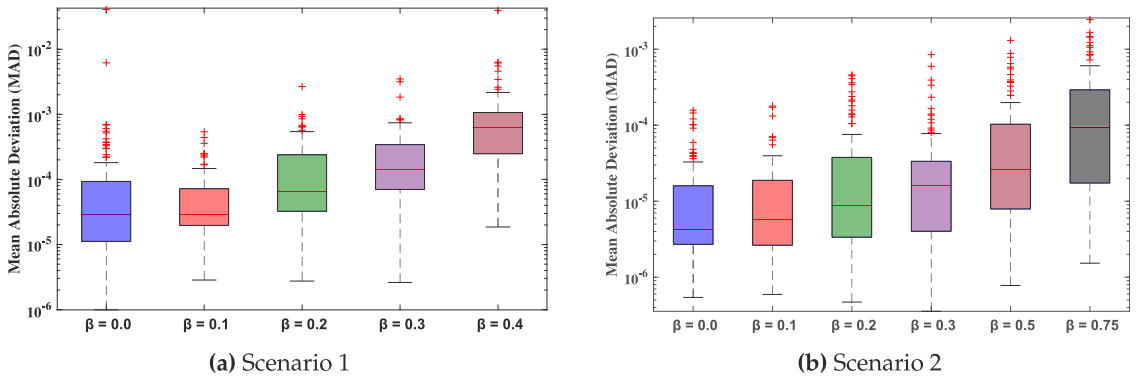

Fig. 10. Graphical analysis of mean absolute deviations obtained by proposed ANN-AOA-AS paradigm for different variations of applied voltage in scenarios 1 and 2.

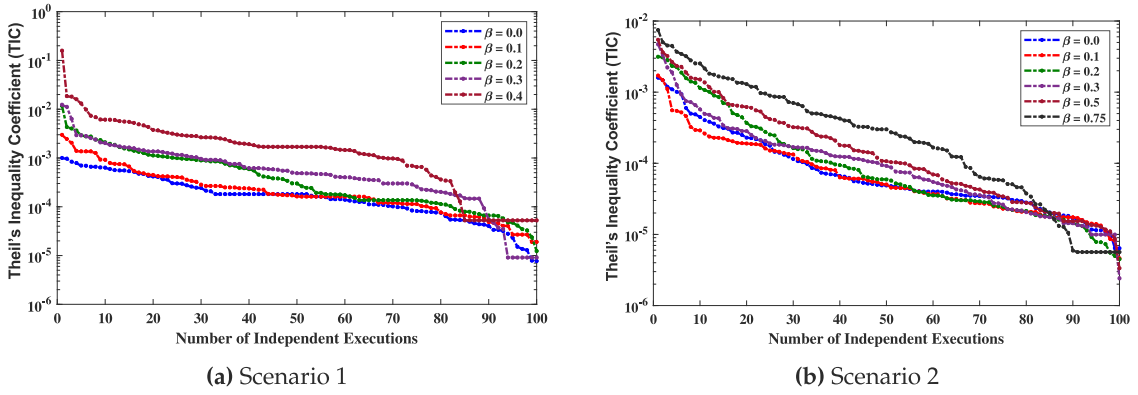

Fig. 11. Convergence of Error in Nash–Sutcliffe Efficiency.

Table 8
Statistical analysis based on minimum (Min), mean and standard deviations (Std) for the performance indices based on the solutions of different cases in scenario 1 and 2.

	Fit			MAD			TIC			RMSE			ENSE		
	Min	Mean	Std	Min	Mean	Std	Min	Mean	Std	Min	Mean	Std	Min	Mean	Std
$\beta = 0.0$	1.38E−09	9.12E−06	7.57E−05	9.93E−07	5.62E−04	4.11E−03	7.71E−06	2.36E−04	2.24E−04	1.12E−06	3.43E−05	3.25E−05	1.61E−08	3.36E−05	6.15E−05
$\beta = 0.1$	8.34E−09	5.71E−06	1.90E−05	2.85E−06	6.41E−05	8.91E−05	1.90E−05	3.52E−04	4.92E−04	3.75E−06	6.93E−05	9.64E−05	7.23E−08	1.06E−04	3.42E−04
$\beta = 0.2$	1.80E−08	6.02E−06	1.97E−05	2.75E−06	1.91E−04	3.27E−04	1.24E−05	8.05E−04	1.41E−03	3.15E−06	2.03E−04	3.50E−04	4.00E−08	7.52E−04	3.84E−03
$\beta = 0.3$	4.90E−08	6.35E−06	1.93E−05	2.62E−06	2.93E−04	5.08E−04	9.10E−06	1.00E−03	1.77E−03	2.94E−06	3.20E−04	5.53E−04	2.26E−08	1.13E−03	5.29E−03
$\beta = 0.4$	2.03E−08	6.53E−05	3.42E−04	1.86E−05	1.32E−03	4.03E−03	5.26E−05	4.15E−03	1.58E−02	2.15E−05	1.47E−03	4.45E−03	7.14E−07	4.58E−03	1.36E−02
$\beta = 0.0$	7.16E−10	5.35E−06	4.89E−05	5.42E−07	1.63E−05	2.95E−05	6.39E−06	1.69E−04	2.99E−04	6.49E−07	1.72E−05	3.03E−05	9.91E−09	3.81E−05	1.30E−04
$\beta = 0.1$	9.13E−11	6.03E−07	2.03E−06	5.42E−07	1.63E−05	2.95E−05	6.39E−06	1.69E−04	2.99E−04	6.49E−07	1.72E−05	3.03E−05	9.91E−09	3.81E−05	1.30E−04
$\beta = 0.2$	3.84E−10	1.51E−06	4.84E−06	4.71E−07	5.03E−05	9.89E−05	4.49E−06	3.36E−04	6.67E−04	7.14E−07	5.32E−05	1.05E−04	9.91E−09	1.68E−04	5.24E−04
$\beta = 0.3$	1.36E−09	7.10E−06	5.19E−05	3.56E−07	4.83E−05	1.16E−04	2.41E−06	2.69E−04	6.42E−04	4.58E−07	5.07E−05	1.20E−04	1.22E−09	1.50E−04	7.88E−04
$\beta = 0.5$	1.00E−08	2.16E−05	1.86E−04	7.79E−07	1.09E−04	2.07E−04	3.35E−06	4.52E−04	8.57E−04	8.61E−07	1.16E−04	2.18E−04	3.17E−09	2.85E−04	1.07E−03
$\beta = 0.75$	2.99E−08	4.44E−05	2.92E−04	1.53E−06	2.55E−04	4.15E−04	5.65E−06	7.76E−04	1.26E−03	2.02E−06	2.74E−04	4.43E−04	6.35E−09	6.40E−04	2.03E−03

CRediT authorship contribution statement

Naveed Ahmad Khan: Software, Methodology, Investigation, Formal analysis, Conceptualization. **Muhammad Sulaiman:** Formal analysis, Methodology. **Benzhou Lu:** Formal analysis, Methodology, Software, Supervision, Writing – review & editing.

Declaration of competing interest

Authors of this manuscript declare that they have no conflict of interest regarding this manuscript.

Data availability

Data will be made available on request.

Appendix

Approximate series solution for scenario 1 and 2 with $\beta = 0.0$ can be regenerated by the following equations

$$y(x) = \left\{ \begin{array}{l} \frac{2.539922402}{1+e^{-(0.599136623x-1.078518289)}} + \frac{0.954826132}{1+e^{-(0.149042982x-2.064023527)}} \\ + \frac{-0.923265472}{1+e^{-(1.306843218x-2.214113229)}} + \frac{-7.410063942}{1+e^{(-1.497063179x-5.638379657)}} \\ + \frac{8.043156465}{1+e^{-(-1.738402506x-4.486117318)}} + \frac{1.009252339}{1+e^{-(1.20364016x+0.45408639)}} \\ + \frac{1.096567955}{1+e^{-(3.066802587x-9.330722844)}} + \frac{0.60999106}{1+e^{(0.176795327x-2.006129937)}} \\ + \frac{-2.092392395}{1+e^{-(1.004441501x+1.086026979)}} + \frac{1.329198614}{1+e^{-(0.119699038x-2.061056991)}}, \end{array} \right. \tag{A.1}$$

$$y(x) = \left\{ \begin{array}{l} \frac{-0.175937013}{1+e^{-(-1.000711433x-0.011809234)}} + \frac{-5.460129533}{1+e^{-(1.482370509x+4.165811435)}} \\ + \frac{-0.172311409}{1+e^{-(-1.002725979x-0.009226097)}} + \frac{4.444384753}{1+e^{(-0.866856148x+3.603274403)}} \\ + \frac{-0.168330066}{1+e^{-(-1.00874048x-0.016097407)}} + \frac{-0.177055609}{1+e^{-(-1.003989768x-0.006383731)}} \\ + \frac{-0.151043635}{1+e^{-(-1.012112995x-0.031358063)}} + \frac{4.366979801}{1+e^{(1.417323413x-5.241288475)}} \\ + \frac{1.20079979}{1+e^{-(-1.163413197x-2.848945378)}} + \frac{5.351318904}{1+e^{-(0.047612713x-1.056330069)}}, \end{array} \right. \tag{A.2}$$

References

Abadyan, M., Novinzadeh, A., Kazemi, A., 2010. Approximating the effect of the Casimir force on the instability of electrostatic nano-cantilevers. Phys. Scr. 81 (1), 015801.

Abdi, J., Koochi, A., Kazemi, A., Abadyan, M., 2011. Modeling the effects of size dependence and dispersion forces on the pull-in instability of electrostatic cantilever NEMS using modified couple stress theory. Smart Mater. Struct. 20 (5), 055011.

Abualigah, L., Diabat, A., Mirjalili, S., Abd Elaziz, M., Gandomi, A.H., 2021. The arithmetic optimization algorithm. Comput. Methods Appl. Mech. Engrg. 376, 113609.

Adel, W., Deniz, S., Approximate solution of the electrostatic nanocantilever model via optimal perturbation iteration method. Comput. Math. Methods Med. e1189.

Akbari, M., Nimafar, M., Ganji, D., Chalmiani, H.K., 2017. Investigation on non-linear vibration in arched beam for bridges construction via AGM method. Appl. Math. Comput. 298, 95–110.

Amorim, T.D., Dantas, W.G., Gusso, A., 2015. Analysis of the chaotic regime of MEMS/NEMS fixed–fixed beam resonators using an improved 1DOF model. Nonlinear Dyn. 79 (2), 967–981.

Batra, R., Porfiri, M., Spinello, D., 2007. Review of modeling electrostatically actuated microelectromechanical systems. Smart Mater. Struct. 16 (6), R23.

Batra, R., Porfiri, M., Spinello, D., 2008. Reduced-order models for microelectromechanical rectangular and circular plates incorporating the casimir force. Int. J. Solids Struct. 45 (11–12), 3558–3583.

Cui, Y., Hong, Y., Khan, N.A., Sulaiman, M., 2021. Application of soft computing paradigm to large deformation analysis of cantilever beam under point load. Complexity 2021.

Fazli, N., Koochi, A., Kazemi, A.S., Abadyan, M., 2014. Influence of electrostatic force and the van der waals attraction on the pull-in instability of the CNT-based probe–actuator. Can. J. Phys. 92 (9), 1047–1057.

Goldberg, N., Leyffer, S., 2015. An active-set method for second-order conic-constrained quadratic programming. SIAM J. Optim. 25 (3), 1455–1477.

Guo, F., Rogerson, G., 2003. Thermoelastic coupling effect on a micro-machined beam resonator. Mech. Res. Commun. 30 (6), 513–518.

Gurtin, M.E., Ian Murdoch, A., 1975. A continuum theory of elastic material surfaces. Arch. Ration. Mech. Anal. 57 (4), 291–323.

Gurtin, M.E., Murdoch, A.I., 1978. Surface stress in solids. Int. J. Solids Struct. 14 (6), 431–440.

Herişanu, N., Marinca, V., 2010. Explicit analytical approximation to large-amplitude non-linear oscillations of a uniform cantilever beam carrying an intermediate lumped mass and rotary inertia. Meccanica 45 (6), 847–855.

Herisanu, N., Marinca, V., 2018. Optimal homotopy asymptotic method to large post-buckling deformation of MEMS. In: MATEC Web of Conferences, vol. 148, EDP Sciences, p. 13003.

Hosseini, I.I., Zand, M.M., Lotfi, M., 2017. Dynamic pull-in and snap-through behavior in micro/nano mechanical memories considering squeeze film damping. Microsyst. Technol. 23 (5), 1423–1432.

Hristov, D., Fallone, B., 1997. An active set algorithm for treatment planning optimization. Med. Phys. 24 (9), 1455–1464.

Huang, W., Jiang, T., Zhang, X., Khan, N.A., Sulaiman, M., 2021. Analysis of beam-column designs by varying axial load with internal forces and bending rigidity using a new soft computing technique. Complexity 2021.

Ke, C., 2006. HD espinosa nanoelectromechanical systems (NEMS) and modeling. In: nd W. Schommers, M.R., Gennes, P.D. (Eds.), Handbook of Theoretical and Computational Nanotechnology. 121, American Scientific Publishers Ch, Illinois, p. 1.

Khan, N.A., Alshammari, F.S., Romero, C.A.T., Sulaiman, M., Laouini, G., 2021a. Mathematical analysis of reaction–diffusion equations modeling the Michaelis–Menten kinetics in a micro-disk biosensor. Molecules 26 (23), 7310.

Khan, N.A., Alshammari, F.S., Romero, C.A.T., Sulaiman, M., Mirjalili, S., 2021b. An optimistic solver for the mathematical model of the flow of Johnson Segalman fluid on the surface of an infinitely long vertical cylinder. Materials 14 (24), 7798.

Khan, N.A., Sulaiman, M., Aljohani, A.J., Bakar, M.A., et al., 2022a. Mathematical models of CBSC over wireless channels and their analysis by using the lenn-WOA-NM algorithm. Eng. Appl. Artif. Intell. 107, 104537.

Khan, N.A., Sulaiman, M., Kumam, P., Alarfaj, F.K., 2022b. Application of Legendre polynomials based neural networks for the analysis of heat and mass transfer of a non-Newtonian fluid in a porous channel. Adv. Continuous Discret. Model. 2022 (1), 1–32.

Khan, N.A., Sulaiman, M., Kumam, P., Bakar, M.A., 2021c. Thermal analysis of conductive-convective-radiative heat exchangers with temperature dependent thermal conductivity. IEEE Access 9, 138876–138902.

Khan, N.A., Sulaiman, M., Lu, B., 2024. Predictive insights into nonlinear nanofluid flow in rotating systems: a machine learning approach. Eng. Comput. 1–18.

Khan, N.A., Sulaiman, M., Tavera Romero, C.A., Alarfaj, F.K., 2021d. Theoretical analysis on absorption of Carbon Dioxide (CO2) into solutions of Phenyl Glycidyl Ether (PGE) using nonlinear autoregressive exogenous neural networks. Molecules 26 (19), 6041.

Koochi, A., Sedighi, H.M., Abadyan, M., 2014. Modeling the size dependent pull-in instability of beam-type NEMS using strain gradient theory. Lat. Am. J. Solids Struct. 11, 1806–1829.

Künzig, T., Niessner, M., Wachutka, G., Schrag, G., Hammer, H., 2010. The effect of thermoelastic damping on the total Q-factor of stateof-the-art MEMS gyroscopes with complex beam-like suspensions. Procedia Eng. 5, 1296–1299.

Liem, A.T., Ari, A.B., McDaniel, J.G., Ekinci, K.L., 2020. An inverse method to predict nems beam properties from natural frequencies. J. Appl. Mech. 87 (6), 061002.

Lim, C.W., 2010. On the truth of nanoscale for nanobeams based on nonlocal elastic stress field theory: equilibrium, governing equation and static deflection. Appl. Math. Mech. 31 (1), 37–54.

Noghrehabadi, A., Beni, Y.T., Koochi, A., Kazemi, A.S., Yekrangi, A., Abadyan, M., Abadi, M.N., 2011. Closed-form approximations of the pull-in parameters and stress field of electrostatic cantilever nano-actuators considering van der Waals attraction. Procedia Eng. 10, 3750–3756.

Osterberg, P.M., 1995. Electrostatically actuated microelectromechanical test structures for material property measurement (Ph.D. thesis). Massachusetts Institute of Technology.

Ozdemir Ozgumus, O., Kaya, M., 2010. Vibration analysis of a rotating tapered Timoshenko beam using DTM. Meccanica 45 (1), 33–42.

Pelesko, J.A., Bernstein, D.H., 2002. Modeling mems and nems. CRC Press.

Phan, D.T., Ghosh, S., 2016. Predicting and mitigating congestion for an electric power system under load and renewable uncertainty. In: 2016 American Control Conference. ACC, IEEE, pp. 6791–6796.

Radi, E., Bianchi, G., Nobili, A., 2021. Bounds to the pull-in voltage of a MEMS/NEMS beam with surface elasticity. Appl. Math. Model. 91, 1211–1226.

Ramezani, A., Alasty, A., Akbari, J., 2008. Analytical investigation and numerical verification of Casimir effect on electrostatic nano-cantilevers. Microsyst. Technol. 14 (2), 145–157.

Rodriguez, A.W., Capasso, F., Johnson, S.G., 2011. The casimir effect in microstructured geometries. Nat. Photonics 5 (4), 211–221.

Timoshenko, S., Woinowsky-Krieger, S., et al., 1959. Theory of plates and shells, vol. 2, McGraw-hill New York.

Wang, G.-F., Feng, X.-Q., 2009. Surface effects on buckling of nanowires under uniaxial compression. Appl. Phys. Lett. 94 (14), 141913.

Wang, X., Pardalos, P.M., 2017. A modified active set algorithm for transportation discrete network design bi-level problem. J. Global Optim. 67 (1), 325–342.

Wen-Hui, L., Ya-Pu, Z., 2003. Dynamic behaviour of nanoscale electrostatic actuators. Chin. Phys. Lett. 20 (11), 2070.

Yaghoobi, H., Valipour, M.S., Fereidoon, A., Khoshnevisrad, P., 2014. Analytical study on post-buckling and nonlinear free vibration analysis of FG beams resting on nonlinear elastic foundation under thermo-mechanical loadings using VIM. Steel Compos. Struct 17 (5), 753–776.

Zare, F., Heydari, M., Loghmani, G.B., Wazwaz, A.-M., 2017. Numerical investigation of the beam-type nano-electrostatic actuator model by using the Birkhoff interpolation method. Int. J. Appl. Comput. Math. 3 (1), 129–146.

Zhang, X., Göhlich, D., Zheng, W., 2017. Karush–Kuhn–Tuckert based global optimization algorithm design for solving stability torque allocation of distributed drive electric vehicles. J. Franklin Inst. 354 (18), 8134–8155.